



J. Serb. Chem. Soc. 78 (11) 1671–1688 (2013)
JSCS–4526

REVIEW

Super-resolution fluorescence imaging and correlation spectroscopy: principles and examples of application

TIJANA JOVANOVIĆ-TALISMAN^{1,2} and VLADANA VUKOJEVIĆ^{3*}

¹Department of Molecular Medicine, Beckman Research Institute of the City of Hope Comprehensive Cancer Center, Duarte, CA 91010, USA, ²Department of Chemistry, University of Hawaii at Manoa, Honolulu, Hawaii 96822, USA and ³Department of Clinical Neuroscience, Karolinska Institutet, CMM L8:01, Stockholm, Sweden

(Received 15 August, revised 30 September 2013)

Abstract: Self-organization of cell-surface receptors in structurally distinct domains in the plasma membrane is of vital importance for correct cellular signaling. However, this dynamic process is difficult to study in cells with sufficiently high temporal and spatial resolution. Herein, two quantitative high-resolution methods with single-molecule sensitivity are presented, *i.e.*, fluorescence correlation spectroscopy (FCS) and pair-correlation photo-activated localization microscopy (pcPALM), which enable the non-destructive study of receptor diffusion and lateral organization at the nanoscale level. The methods are introduced and their application in studies of lateral organization of G protein-coupled receptors (GPCRs) is reviewed. Examples from studies on the lateral organization of opioid receptors are presented in order to illustrate the most recent advances in the field.

Keywords: fluorescence correlation spectroscopy, super-resolution fluorescence imaging, sub-diffraction limit, photo-activated localization microscopy, G protein-coupled receptors, lipid rafts.

CONTENTS

1. INTRODUCTION
2. FLUORESCENCE CORRELATION SPECTROSCOPY (FCS)
 - 2.1. FCS measurements and data analysis
 - 2.2. Probing the lateral organization in the plasma membrane at the nanoscale level by varying spatial scales FCS
 - 2.3. Limitations of FCS
3. PHOTO-ACTIVATED LOCALIZATION MICROSCOPY (PALM) AND PAIR-CORRELATION PALM (PCPALM)
 - 3.1. Limitations of PALM and pcPALM

* Corresponding author. E-mail: vladana.vukojevic@ki.se
doi: 10.2298/JSC130815102J

4. GPCR LATERAL ORGANIZATION INVESTIGATED BY FCS AND PALM

5. CONCLUSIONS

1. INTRODUCTION

Lateral diffusion of cell surface receptors and receptor sorting into specific compartments in the plasma membrane play an essential role in cell signal transduction.^{1–7} Plasma membrane compartmentalization arises spontaneously, due to the natural tendency of lipids to separate into distinct liquid-ordered (L_o) or liquid-disordered (L_d) phases, forming submicroscopic domains where certain lipids (such as cholesterol and sphingolipids) and proteins can be concentrated while others can be excluded. The thus formed L_o submicroscopic domains, frequently referred to as lipid rafts, are believed to participate in a number of vital cellular functions.^{1–7} In spite of intense research that followed the original proposition of these domains,¹ *in vivo* existence of lipid rafts and their biological role remained difficult to confirm for many years. The main obstacle was the limitation of experimental techniques that were available for quantitative characterization of these dynamic structures under non-destructive (living cells) or minimally invasive (fixed cells) conditions.

To date, fluorescence microscopy imaging and spectroscopy techniques have provided compelling evidence for the existence of lateral heterogeneity of protein and lipid organization in intact cell membranes.^{8–22} The aim of this paper is to present two quantitative methods with single-molecule sensitivity, fluorescence correlation spectroscopy (FCS) and pair-correlation photo-activated localization microscopy (pcPALM), and review their application for the study of lateral organization of G protein-coupled receptors (GPCRs). Examples from studies on opioid receptors are used to illustrate how concomitant application of these specialized techniques enables the quantitative characterization of the surface density, lateral diffusion in living cells and heterogeneous distribution in intact plasma membranes of opioid receptors at the nanoscale level.

2. FLUORESCENCE CORRELATION SPECTROSCOPY (FCS)

FCS is a quantitative method with single molecule-sensitivity that uses statistical analysis of fluorescence intensity fluctuations recorded over time to obtain information about molecular numbers and their transporting properties and/or molecular brightness distribution.^{23–25} The principles of FCS were formulated about thirty years ago,^{26–30} and the method was successfully applied for in solution studies of molecular diffusion and kinetics in the founding laboratories. More widespread application in biological systems became possible only after confocal optical arrangement and ultra-sensitive avalanche photodiode (APD) detectors were implemented.^{31,32} Application of these innovations significantly improved the signal-to-noise ratio, enabling single-molecule detection sensitivity, low excitation intensities and short measurement times. Building on these

innovations, second and third generations of versatile instruments that combined FCS with confocal laser scanning microscopy (CLSM) were developed,^{33,34} which paved the way for a more widespread use of FCS in biomedical research. FCS measurements on live PC12 cells stably transformed to express mu-opioid receptors fused with the enhanced Green Fluorescent Protein (MOP^{eGFP}) are shown as an example (Fig. 1 B). A schematic presentation of a typical FCS–CLSM setup is given in Fig. 1A. To induce fluorescence, the sample is illuminated by incident light delivered by a continuous wave laser. The laser beam is reflected by a dichroic mirror and sharply focused by the objective to form a mini-

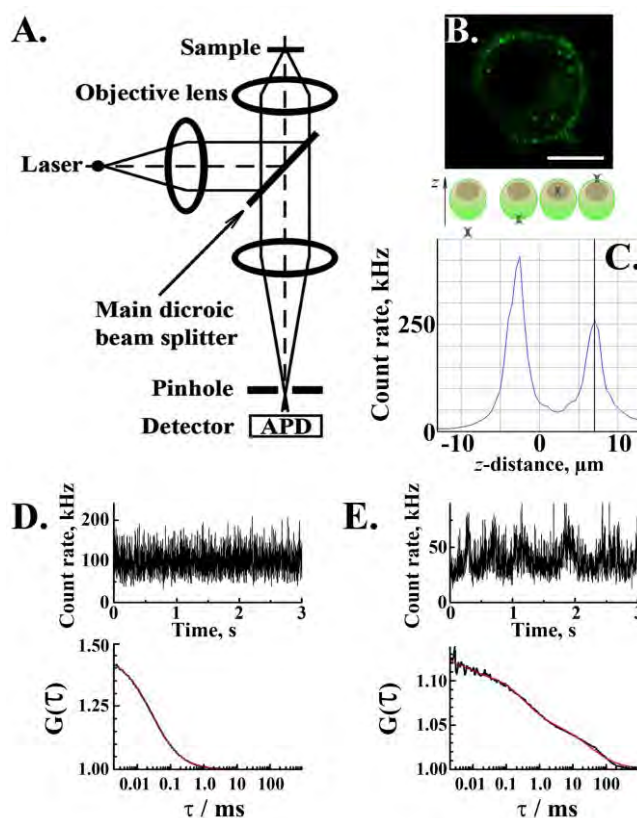


Fig. 1. FCS measurements and data analysis. A. Schematic drawing of a typical FCS/CLSM setup. B. Confocal image of a single PC12 cell stably expressing MOP^{eGFP} (green), acquired using APD. Scale bar: 5 μm . C. Fluorescence intensity distribution across a single PC12 cell expressing MOP^{eGFP} determined by a linear scan in the axial direction (z -scan). The first and second maximums indicate the position of the basal and apical plasma membrane, respectively, as schematically depicted in the panel above. D and E. Fluorescence intensity fluctuations (top) and corresponding autocorrelation curves (bottom) recorded in a standard solution of rhodamine 6G (Rho6G) in water (D) and on the apical plasma membrane of a single PC12 cell expressing MOP^{eGFP} (E).

ature volume element, the size of which is determined by the diffraction of light. The volume from which fluorescence is detected is further reduced by a pinhole (confocal aperture) in the image plane, rejecting stray and out of focus light and keeping the Raman scattered light to a minimum. In this way, fluorescence is detected from a minute observation volume element that is about $2 \times 10^{-19} \text{ m}^3$. This enables a submicrometer resolution and specific detection at defined loci, as well as quantitative and background-free analysis. The light emitted by fluorescing molecules passing through the confocal volume element is separated from the exciting radiation and the scattered light by a dichroic mirror and barrier filter, and transmitted to the single-photon avalanche photodiode (APD) detector, which responds with an electrical pulse to each detected photon. The number of pulses originating from the detected photons, recorded during a specific time interval, corresponds to the measured light intensity. Thus, in one FCS experiment, changes in fluorescence intensity in time are registered. The eGFP fluorescence was excited using the 488 nm line of an Ar/ArKr laser. The main dichroic beam splitter HFT KP 700/488 was used to separate the incident and emitted light. The emitted light was further spectrally selected using a band pass filter BP 505–530 nm in front of the APD detector (Fig. 1B). Autocorrelation analysis showed that the average number of Rho6G molecules in the observation volume element was 2.3 (meaning that one typically observes 2 ($\approx 67\%$ of the time) or 3 ($\approx 33\%$ of the time) Rh6G molecules simultaneously, Fig. 1D and E), whereas the average number of observed MOPeGFP molecules is 9.2. The number of detected photons per molecule and second in Rh6G aqueous solution was $\text{CPMRho6G} = 41.9 \text{ kHz}$, yielding a virtually noise-less autocorrelation curve (black in Fig. 1C and D) that is well fitted with the autocorrelation function for free 3D diffusion and singlet/triplet transition of a single component (red in Fig. 1D and E). In contrast, the eGFP brightness is an order of magnitude lower, $\text{CPMMOPeGFP} = 3.8 \text{ kHz}$. The experimental autocorrelation curve is complex, showing several characteristic times (black in Fig. 1D and E), and could be well fitted using an autocorrelation function for free 2D diffusion and singlet/triplet transition of two components (red curve, see Eq. (2)).

2.1. FCS measurements and data analysis

In studies of protein lateral organization in plasma membranes by FCS, live cells genetically modified to express the receptor of interest fused with a fluorescent protein marker are typically used.^{18,19,35,36} This is somewhat disadvantageous for FCS because the quantum yield of fluorescent proteins is typically smaller than those of organic fluorophores or quantum dots, which necessitates longer measurement times. However, an obvious advantage of genetic labeling is that it obviates artifacts associated with covalent protein labeling and/or protein organization disruption due to multiple crosslinking with antibodies.

Before an FCS measurement can be initiated, confocal imaging is used to identify cells suitable for FCS analysis. For example, a confocal image of PC12 cells stably transformed to express the mu-opioid receptor fused with an enhanced green fluorescent protein (MOP^{eGFP}) is shown in Fig. 1B. When a suitable cell has been identified, which does not have another cell on top of it and is not too bright (overexpression of proteins can introduce artifacts in their lateral organization), fluorescence intensity scanning is performed in the axial direction (a so-called *z*-scan) to localize the apical plasma membrane of the cell (schematically depicted above Fig. 1C). A fluorescence intensity profile generated in this way is shown in Fig. 1C. Thereafter, continuous wave laser light is delivered to a small area in the plasma membrane, and fluctuations in fluorescence intensity are recorded as a function of time (Fig. 1 D and E, top).

To evaluate the gathered data, *i.e.*, to analyze time series sampled during one run, statistical methods are applied to detect non-randomness in the data. Typically, this is realized by temporal autocorrelation analysis, but other methods such as higher order autocorrelation functions,^{37,38} fluorescence intensity distribution analysis (FIDA),^{39,40} photon-counting histograms (PCH),^{41,42} fluorescence cumulant analysis (FCA),⁴³ and time-integrated fluorescence cumulant analysis (TIFCA)^{44,45} can be also applied. However, the temporal autocorrelation analysis of fluorescence intensity fluctuations is still the most frequently used method in FCS applications.

In temporal autocorrelation analysis, the normalized autocorrelation function $G(\tau)$ is first derived:

$$G(\tau) = 1 + \frac{\langle \delta I(t) \delta I(t + \tau) \rangle}{\langle I(t) \rangle^2} \quad (1)$$

that relates the fluctuation in fluorescence intensity measured at a certain time point t , $\delta I(t) = I(t) - \langle I(t) \rangle$, which is given as the difference in fluorescence intensity $I(t)$ and the mean fluorescence intensity over the recorded time-series ($\langle I(t) \rangle$), and its intensity measured at a later time, $\delta I(t + \tau) = I(t + \tau) - \langle I(t) \rangle$. For further analysis, $G(\tau)$ is plotted as a function of different lag times τ , also called autocorrelation times, to construct the corresponding autocorrelation curve (Fig. 1D and E, bottom). In molecular systems undergoing stochastic fluctuations, random variations of $G(\tau)$ around the value $G(\tau) = 1$ would be observed. For processes that are not random, an autocorrelation curve builds up with a maximal limiting value of $G(\tau)$ as $\tau \rightarrow 0$, decreasing to the value of $G(\tau) = 1$ at long times, indicating that correlation between the initial and the current property value has been lost. For simple systems, with only one chemical species and one process that underlie the fluorescence intensity fluctuations, autocorrelation curves with only one characteristic time are observed (Fig. 1D, bottom). In complex systems, where more than one process underlies the fluorescence intensity

fluctuations, or chemical species with different diffusion times exist, more than one characteristic time could be observed if the processes are sufficiently well separated in time (Fig. 1E, bottom).

To obtain information about the average number of molecules observed, the so-called non-uniform part of the normalized autocorrelation function is used, $g(\tau) = G(\tau) - 1$. In this case, one observes a maximal limiting value of $g(\tau)$ as $\tau \rightarrow 0$ is observed that decreases to the value of $g(\tau) = 0$ at long times. The limiting value of $g(\tau)$, as $\tau \rightarrow 0$ is then inversely proportional to the absolute concentration of the fluorescing molecules. Both the normalized autocorrelation function $G(\tau)$ and its non-uniform part $g(\tau)$ are independent of the properties of the experimental setup, such as the laser intensity, fluorescence quantum yield and detection efficiency.²³ A comprehensive description of autocorrelation analysis and the derivation of the autocorrelation function for the simplest case, free three-dimensional (3D) diffusion in an isotropic medium, can be found at <http://www.biotech.tu-dresden.de/cms/index.php?id=151>.⁴⁶ Here, only the most relevant results for lateral diffusion (two-dimensional (2D) diffusion in a plane) are given.

To extract the information about molecular numbers (N) and lateral diffusion times (τ_D), the experimental autocorrelation curves are fitted using autocorrelation functions derived for the appropriate model system.²³ For measurements performed at a plasma membrane, a model for free 2D diffusion with triplet contribution is typically used:

$$G(\tau) = 1 + \frac{1}{N} \left(\sum_i \frac{x_i}{(1 + \tau/\tau_{Di})} \right) \left(1 + \frac{T}{1-T} \exp\left(-\frac{\tau}{\tau_T}\right) \right) \quad (2)$$

In Eq. (2), T is the average equilibrium fraction of molecules in the triplet state, τ_T is the relaxation time of the triplet state, i is the number of components, τ_{Di} is the diffusion time of the i -th component and x_i is its relative amplitude ($\sum x_i = 1$). The diffusion times, τ_{Di} , of the investigated components are determined from the autocorrelation function (2) that best matches the actual, experimentally determined autocorrelation curve.

The diffusion time, τ_D , is related to the translation diffusion coefficient, D , through the relationship:

$$\tau_D = \frac{w_{xy}^2}{4D} \quad (3)$$

where w_{xy} is the so-called lateral radius, *i.e.*, the radial distance of the focused laser beam at which the collected fluorescence intensity has dropped by a factor of e^2 compared to its peak value in the center. This parameter is derived in calibration measurements, using standard aqueous solutions of fluorescent molecules the diffusion coefficients of which are known. For this purpose, the fluores-

cent properties of the standard dye need to match the properties of the fluorescent protein, and identical optical settings have to be applied for FCS measurements (Fig. 1D and E). Diffusion coefficients of organic fluorophores typically used as reference standards in FCS can be found at http://www.picoquant.com/tech-notes/appnote_diffusion_coefficients.pdf.⁴⁷ The lateral radius w_{xy} depends on the instrumental setting, but the theoretical limit for a diffraction-limited spot size gives a range from 200–270 nm for typically used excitation wavelengths 488–633 nm.

Thus, FCS examines a small area ($(w_{xy})^2\pi$) in the plasma membrane that is limited in size by the diffraction of light and the quality of the optics. It provides quantitative information about the local density of cell surface receptors and the lateral diffusion in the observed area in living cells. Even though the spatial resolution of FCS is limited by light diffraction, FCS can give information about the structural organization at the nanoscale level, *i.e.*, beyond the spatial resolution limit that is imposed by diffraction of light, as will be shown later.

2.2. Probing the lateral organization in the plasma membrane at the nanoscale level by varying spatial scales FCS

Lateral heterogeneity and the presence of microdomains affect the diffusion behavior of molecules composing the plasma membrane. However, long-range diffusion measurements, such as fluorescence recovery after photobleaching (FRAP), which is the most widely used technique for measuring molecular diffusion in cellular membranes, have largely failed to recognize such differences. The main reason for this is that FRAP measurements are typically conducted on an ensemble of molecules, such that individual behavior of molecules cannot be distinguished. Owing to the high temporal resolution and single molecule sensitivity of FCS, it was recently shown that FCS measurements performed at varying spatial scales can provide information about local differences in the diffusion properties of cell-surface receptors in the plasma membrane.^{48–52} Using this method, three models of diffusion could be distinguished by plotting the lateral diffusion time (τ_D) as a function of the observation area size, which is proportional to $(w_{xy})^2$, and determining the intercept for a vanishingly small observation area (Fig. 2A). A positive intercept was associated with partitioning in domains as the predominant mode of lateral organization, free diffusion yielded a zero intercept, and a negative intercept reflected receptor confinement by the cytoskeletal meshwork.^{48–52}

To corroborate this remarkable observation, single nanometric apertures of different sizes were combined with FCS to reduce the size of the observation area from which photons are collected and thus achieve the high spatial resolution that is necessary to characterize the underlying structures at the nanoscale level.⁵³ This approach verified the previous observations that FCS can give information

about structures that are smaller in size than the spatial resolution limit that is imposed by light diffraction.^{48–52} FCS at varying spatial scales was also shown to be superior to single particle tracking (SPT) because of the high temporal resolution, high sampling and the robust autocorrelation analysis that is much simpler than the tedious analysis of large numbers of individual trajectories, which is necessary for the accurate interpretation of SPT results.

The experimentally derived dependence of the autocorrelation time for MOPe^{GFP} as a function of the size of the observation area is shown in Fig. 2B. The positive intercept suggests that opioid receptors partition between microdomains and the surrounding lipid bilayer.

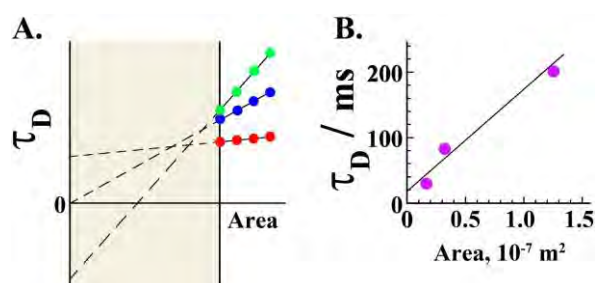


Fig. 2. Probing the lateral organization in the plasma membrane at the nanoscale level by varying spatial scales FCS. A. Lateral diffusion time as a function of the size of the observation area for different types of lateral organization in the plasma membrane: a network of barriers defining contiguous corrals (green), free diffusion (blue) and isolated domains (red), derived by numerical simulations according to the so-called FCS diffusion law.^{48–53} The shaded region indicates observation areas that are smaller in size than the area defined by diffraction of light. Direct FCS measurements in this domain cannot be performed by classical FCS, but the behavior can be inferred by extrapolation (dashed line) of the data set collected for areas that are larger in size than the diffraction limited area (solid line). B. Experimentally measured dependence of the lateral diffusion time of opioid receptors in live cells as a function of the observation area size. The size of the observation volume element was changed by changing the pinhole size (ph) in front of the detector. The observed area, expressed as $(ph)^2\pi$, is proportional to the actual observation area.

2.3. Limitations of FCS

Endogenous non-fluorescent protein molecules, protein constructs with irreversibly photobleached fluorophores or with fluorophores residing in dark states, and proteins associated with large immobile structures will all be invisible for FCS and will lead to an underestimation of the receptor surface density. Irreversible photobleaching of fluorophores may also induce errors in the measurements of the lateral diffusion time, yielding shorter values of τ_D , and hence larger diffusion coefficients. To avoid artifacts due to photobleaching, the incident laser intensity used for FCS measurements needs to be as low as possible. The appropriate laser intensity is usually selected so that the detected number of photons

per molecule and second, so-called count per molecule, is not lower than 1 kHz (to ensure that the measured signal is coming from the fluorophore, rather than from autofluorescent molecules abundant in the cell), and the lateral diffusion time does not increase when the laser intensity is reduced.

FCS gives a dynamic readout, yielding characteristic times of processes underlying fluorescence intensity fluctuations. However, its localization precision is poor – FCS can localize the receptor in the plasma membrane with an uncertainty that is limited by the diffraction of light, which is about ± 200 nm at best. To visualize a receptor and determine its localization with greater precision, super-resolution fluorescence imaging techniques are required.

3. PHOTO-ACTIVATED LOCALIZATION MICROSCOPY (PALM) AND PAIR-CORRELATION PALM (pcPALM)

Reconstruction based super-resolution fluorescence microscopy imaging techniques such as photo-activated localization microscopy (PALM),⁵⁴ stochastic optical reconstruction microscopy (STORM)⁵⁵ and fluorescence photo-activation localization microscopy (fPALM)⁵⁶ use repetitive activation and imaging of single fluorophores. This process is reiterated over several minutes (tens of thousands of frames are typically acquired) allowing single fluorophores to be generally positioned with respect to one another at distances greater than the diffraction limit in any particular frame. The centers of the peaks are mathematically calculated for each frame based on the photon distribution from single fluorophores, and all frames are added together. This approach yields pointillistic images, where individual molecules can be localized with a high precision, typically 15–40 nm.^{21,22,54–61} The principles of reconstruction based super-resolution fluorescence microscopy imaging techniques were primarily defined in the seminal works of Michalet *et al.*,⁵⁷ Thompson *et al.*,⁵⁸ Yildiz *et al.*⁵⁹ and Betzig *et al.*,⁵⁴ in which it was shown that the fluorescence intensity, *i.e.*, the number of detected photons, determines the precision by which a single molecule can be localized. By showing that the accuracy of single molecule localization depends on the width of the point spread function (PSF) and the square root of the collected number of photons (n):

$$\sigma = \frac{\omega_{xy}}{\sqrt{n}} \quad (4)$$

they showed that if $n = 10000$ photons, for a single fluorescing molecule could be detected, $\lambda = 500$ nm ($\omega_{xy} \approx 250$ nm), the molecule could be localized with a precision of ± 1.3 nm.

In order to acquire a sufficient number of photons from a single molecule, which are required for achieving the high localization precision in accordance with Eq. (4), these super-resolution techniques rely on switchable fluorescence reporters, which can cycle to/from a metastable dark state many times, in the case

of photo-activatable fluorophores, or from one color to another in the case of photoconvertible fluorophores. By stochastically activating, localizing, and then photobleaching (in PALM) the switchable fluorescence reporters, a sufficient number of photons can be collected from single molecules, enabling their localization with a high precision.

In order to detect optimally the relatively faint emission from single molecules localized in the plasma membrane, pointillistic imaging techniques use total internal reflection fluorescence (TIRF) to generate an evanescent excitation wave that penetrates 100–200 nm into the specimen, leading to extreme rejection of the background fluorescence (Fig. 3A). The sequence of events for determining the precise location of a single set of photo-activated fluorescent probes, for example the photo-activatable GFP (paGFP)⁶² is as follows. Initially all molecules in the specimen are inactive (native non-emissive state; dark circles). A violet 405 nm laser is used to photo-activate a subset of molecules in the specimen. The number of activated paGFP molecules can be maintained low by ensuring the laser intensity is sufficiently weak at the focal plane. Photo-activation of the molecules occurs stochastically, where the probability of activation is proportional to the intensity of the activation laser. After photo-activation, the 488 nm laser is used to detect and record the position of the photo-activated molecules within the illu-

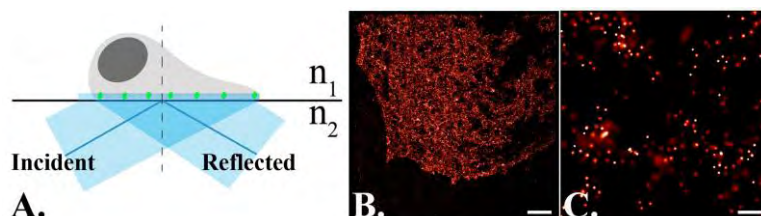


Fig. 3. PALM imaging. A. In order to optimally detect the relatively faint emission from single molecules, PALM uses total internal reflection fluorescence (TIRF) to suppress the background fluorescence. In TIRF, the sample is illuminated at an angle that causes total internal reflection of the incident light at the boundary of the two media. In this way, an evanescent excitation wave is generated that propagates across the boundary surface, penetrating approximately 150 nm into the specimen. TIRF enables the simultaneous imaging of the complete basal plasma membrane, as schematically depicted. B. PALM image of the basal plasma membrane of a Cos7 cell expressing MOP^{paGFP}, showing the localization of individual receptor molecules. Super-resolution images were generated by analyzing the datasets using standard PALM analysis.⁵⁴ The identified peaks were fitted using a cylindrically symmetric Gaussian point spread function, with the amplitude being proportional to the number of photons collected, and the standard deviation (σ) depending on the localization precision. Peaks were grouped using maximum dark time due to blinking of 10 s for paGFP and group radius of $2.5 \times \sigma$ (98.8 % confidence level). The figures are rendered and show the probability to observe a molecule, with white color representing the highest value.

Scale bar: 5 μ m. C. Magnified PALM image showing a detail from the image in B. Scale bar: 200 nm.

minated area. During readout, the photo-activated molecules spontaneously photobleach, eventually reducing the number of active molecules in the specimen. A new set of molecules is photo-activated to repeat the sequence, which is reiterated until all molecules in the specimen have been exhausted.

Typically, 10^3 – 10^5 diffraction-limited digital TIRF images are acquired to yield one super-resolution image; data analysis is performed to identify single molecules over the background noise, calculate the PSFs for the identified single molecules, and determine their centers and localization precision.

Quantitative super-resolution imaging techniques can provide information about nanoscale spatial organization and help delineate mechanisms of various biological processes.^{63–69} For this purpose, statistical methods for spatial analysis, such as the Ripley K-function, the Getis and Francklin L-function or pair correlation function (PCF) are typically used to derive various cluster parameters.^{70,71} Recently developed, pair-correlation PALM (pcPALM) utilizes autocorrelation analysis to separate contributions from a) stochastic clustering (single fluorophores often appear in multiple frames and not sequentially due to variable intervals of fluorescent blinking) and b) protein clustering to provide quantitative information about lateral protein organization. Typically, 2–5 μm wide square regions of interest (ROIs) are selected. The size of the ROI depends on the size of the continuous plasma membrane region of the cell. Generally, a larger ROI and higher number of localized molecules per μm^2 lead to better statistical analyses. The spatial dispersion of identified molecules in the selected ROI is quantified in order to determine whether the investigated molecules are randomly distributed or clustered. For regions that indicate clustering, protein autocorrelation contribution is fit to an exponential function, and pcPALM analysis yields important clustering parameters: cluster size, number of detected proteins in the cluster and increased local density in clusters.

PALM has advantages over FCS because it enables the study of cell surface protein organization with nanoscopic (15–40 nm) precision across the complete basal plasma membrane, rather than in a very small area. For example, the lateral distribution of MOPpaGFP in transiently transformed Cos7 cells is shown in Figs. 3B and C. Furthermore, pcPALM^{21,22} enables the quantitative characterization of the lateral organization of proteins in the plasma membrane in terms of extent of protein clustering, protein density per cluster, and cluster size distributions. Pair-correlation analysis of MOPpaGFP PALM datasets in transiently transformed Cos7 cells is currently under way in our lab. Preliminary results suggest that opioid receptors largely reside in clusters that are smaller than 100 nm in size, characterized by a MOPpaGFP surface density that is several times larger than in the surrounding lipid bilayer. Thus, PALM and pcPALM suggest that MOPpaGFP partitions in domains, which is in line with the FCS results (Fig. 2B).

3.1. Limitations of PALM and pcPALM

Quantitative pointillistic microscopy techniques provide precise information about molecule localization and quantitatively characterize their patterning in the plasma membrane, which yields information about cluster size and protein density per cluster distributions. However, they do not give any information about the molecular dynamics in the plasma membrane. A recently developed technique, single-particle tracking PALM (sptPALM), can be used for dynamics studies in live cells.⁷² In sptPALM, raw data are acquired under continuous activation/excitation while the cells are maintained under physiological conditions. The image of each molecule is fit with a Gaussian to yield nanometric localization precision; molecular positions in consecutive frames are then associated with trajectories based on their proximity, and diffusion parameters are extracted. Points-accumulation-for-imaging-in-nanoscale-topography (PAINT), an earlier method that unifies diffusion with tracking, also provides both high localization precision and dynamic information.⁷³

As in FCS, endogenous non-fluorescent protein molecules and protein constructs with irreversibly photobleached fluorophores will be invisible, yielding an undervalued estimation of total protein surface density by quantitative analysis of pointillistic microscopy data. In contrast, multiple observations of the same protein molecule may cause an overestimation of protein density – photophysical processes leading to a spontaneous molecular transition to/from dark states cause fluorophore blinking, which may be erroneously interpreted as the appearance of another molecule. Statistical methods^{21,22} and proper photophysical characterization of fluorescent probes^{74,75} reduce issues associated with multiple appearances of a single molecules.

4. GPCR LATERAL ORGANIZATION INVESTIGATED BY FCS AND PALM

G protein-coupled receptors (GPCRs), which consist of approximately 800 members, represent one of the largest receptor groups in the metazoa, GPCRs account for approximately 2 % of the coding genes in the human genome and regulate a myriad of physiological processes through the binding of structurally diverse ligands, such as ions, amino acids, biogenic amines, alkaloids and peptides. They are also the largest class of molecular targets with proven therapeutic value: more than 50 % of today's pharmaceuticals target GPCRs. In spite of their great relevance and intensive research, detailed mechanisms of GPCR functions are still not sufficiently understood at the molecular and cellular level. Hence, concerted efforts were embarked on several years ago to unravel crystal structures of GPCRs and identify molecules that modulate their function. This resolute effort has led to the determination of the crystal structure of 16 distinct GPCRs, which was recently reviewed by Katritch *et al.*⁷⁶ In parallel, intensive effort is continuously being dedicated to understanding cellular mechanisms that regulate

the surface density GPCRs and their lateral organization, *i.e.*, oligomerization and sorting to specialized compartments in the plasma membrane.^{77–79} The latter mechanism is of particular interest because it may diversify the GPCR repertoire without the need for creating new genetic protein variants. For many years, receptor oligomerization and sorting to lipid rafts were investigated using standard biochemical techniques. However, these methods are largely disruptive, may introduce artifacts, and do not provide sufficient information about the dynamics of these processes. This, in turn, necessitates live cell studies and the application of minimally invasive techniques, such as high-resolution fluorescence microscopy imaging and correlation spectroscopy.

The earliest FCS studies of GPCR dynamics, interactions in solution,⁸⁰ and interactions on isolated cell membranes⁸¹ date back to 1999, whereas the first application on live cells was reported in 2002.⁸² The same year, FCS was used to characterize the photo-induced oligomerization of bacteriorhodopsin in giant unilamellar vesicles (GUVs), which were identified through the change in the mobility of bacteriorhodopsin upon photo-activation.⁸³ These pioneering studies demonstrated the usefulness of FCS for quantitative characterization of ligand–receptor interactions, which paved the way for future applications. In the past 10 years, numerous studies were dedicated to the quantitative characterization of the lateral organization of different GPCRs in different cell lines. The effect of selective agonists, selective antagonists, and non-specific substances (such as lipids, ions and alcohols (ethanol in particular)) on GPCR surface density, oligomerization status, association with lipid rafts and cellular trafficking have also been studied in detail. In particular, the following representatives of GPCR were investigated: the 5-hydroxytryptamine or serotonin receptor 5-HT_{2A}, adrenergic receptors α_{1b} -AR and β_2 -AR, muscarinic receptors M₁ and M₂, and dopamine receptor D₁ in human embryonic kidney 293 (HEK293) cells;³⁶ bradykinin type 2 receptor B₂R and the mu-opioid receptor MOP in fisher rat thyroid (FRTwt) cells;⁸⁴ serotonin receptor 5-HT_{2C} in HEK293 cells;⁸⁵ neuropeptide Y receptor NPY in HEK293T and HEK293TR cells;⁸⁶ histamine receptor H₁ in chinese hamster ovary (CHO-K1) cells;⁸⁷ serotonin receptor 5-HT_{1A} in CHO-K1 cells;⁸⁸ corticotropin-releasing factor receptors CRFR₁ and CRFR₂ in HEK293 cells;⁸⁹ muscarinic receptors M₁ in HEK293 cells;⁹⁰ MOP in rat Pheochromocytoma (PC12) cells;^{18,19} chemokine receptor 4 (CXCR4) in HEK293;⁹¹ adenosine receptor A₃ in CHO cells;⁹² bradykinin type 2 receptor B₂R in HEK293;⁹³ adenosine receptor A₁ in CHO cells;⁹⁴ and adrenergic receptor β_2 -AR in alveolar epithelial type II (A549) cells and hippocampal neurons.⁹⁵

In comparison, the number of GPCR-dedicated PALM studies is still limited, with only two publications to date, in which the lateral organization of adrenergic receptor β_2 -AR was investigated in HeLa, CHO and cardiomyocyte H9C2 cells.^{64,96} These studies suggested that β_2 -AR is partially pre-associated in nano-

scale-sized clusters only in the cardiomyocyte H9C2 cells, but not in HeLa and CHO cells. Cholesterol sequestration and removal was shown not to affect β_2 -AR clustering, whereas the inhibition of actin polymerization decreased their formation, suggesting that β_2 -AR clustering is influenced by the actin cytoskeleton, and that β_2 -AR is not related to lipid rafts.

5. CONCLUSIONS

Studies of GPCRs lateral organization by FCS^{18,19,36,84–95} revealed that there are significant differences in the lateral organization, dynamics, and selectivity to ligands, modulators, and downstream signaling effectors between the investigated GPCRs. Furthermore, these studies revealed that lateral organization of GPCRs may be cell-type specific, and suggested that differences may persist even in the same subfamily of GPCRs, where different subtypes share a high degree of sequence similarity (> 60 % in the case of opioid receptor subtypes).^{18,19,84}

Hitherto published FCS and pcPALM results support the general notion that the complexity of GPCR lateral organization is vast. However, some unifying concepts seem to be slowly emerging. For example, FCS studies showed that several GPCRs dynamically partition between lipid-enriched domains and the lipid bilayer constituting the plasma membrane. Super-resolution PALM imaging reveals that GPCRs cluster in the plasma membrane, and pcPALM enabled the derivation of important lateral distribution parameters, such as the local cluster density (a unitless number that compares the density of proteins inside and outside the clusters), cluster radius, and number of detected proteins per cluster. Thorough understanding of GPCR lateral organization in the plasma membrane and the dynamical mechanisms that uphold these dissipative structures is essential for a quantitative understanding of GPCRs function, which appears to be finely tuned by the immediate local lipid environment.

The work presented herein demonstrates that FCS and pcPALM are suitable for the quantitative characterization of the spatial heterogeneity GPCRs, and that these methods provide complementary information. PALM offers visual information that is intuitively easy to understand and is of immense value for the interpretation of temporal autocorrelation curves recorded by FCS, which may be challenging at times. Thus, FCS and pcPALM seem to be the methods of choice for quantitative studies of protein organization in cellular plasma membranes, but more standardized approaches in experimental design and data analysis are required to enable future application of these techniques on a larger scale. In spite of these difficulties, which will be resolved in the course of future applications, these techniques hold the promise to bring closer the quantitative characterization of protein–lipid interactions, and their dynamic organization in the plasma membrane.

Acknowledgements. Support from the Karolinska Institute Research Funds, the Ministry of Education, Science and Technological Development of the Republic of Serbia, Grants Nos. 172015 and 45001, and the University of Hawaii at Manoa and City of Hope Startup Funds are gratefully acknowledged. We acknowledge S. Tobin and E. Cacao for the acquisition and analysis of MOPpaGFP data.

ИЗВОД

СУПЕР-РЕЗОЛУЦИОНА ФЛУОРЕСЦЕНТНА МИКРОСКОПИЈА И КОРЕЛАЦИОНА СПЕКТРОСКОПИЈА: ПРИНЦИП РАДА И ПРИМЕНА

ТИЈАНА ЈОВАНОВИЋ-ТАЛИСМАН^{1,2} и ВЛАДАНА ВУКОЈЕВИЋ³

¹*Department of Molecular Medicine, Beckman Research Institute of the City of Hope Comprehensive Cancer Center, Duarte, CA 91010, USA,* ²*Department of Chemistry, University of Hawaii at Manoa, Honolulu, Hawaii 96822, USA* и ³*Department of Clinical Neuroscience, Karolinska Institutet, CMM L8:01, Stockholm, Sweden*

Латерална дифузија и спонтана организација протеинских молекула у суб-микроскопске домене на површини ћелије, су од виталног значаја за правилан пренос сигнала из спољашње средине. У овом раду представљене су квантитативне методе високе осетљивости, флуоресцентна корелациона спектроскопија (енгл. *fluorescence correlation spectroscopy* (FCS)) и корелациона фотоактивациона микроскопија (енгл. *pair-correlation photoactivated localization microscopy* (pcPALM)), које омогућавају да ове динамичке процесе изучавамо са високом временском и просторном резолуцијом. Циљ овог прегледног рада јесте да опише наведене методе и прикаже њихову примену за проучавање латералне организације G-протеин-спрегнутих рецептора (енгл. *G-protein-coupled receptors* (GPCRs)). Резултати наших истраживања латералне организације опијатних рецептора дати су као пример.

(Примљено 15. августа, ревидирано 30. септембра 2013)

REFERENCES

1. K. Simons, E. Ikonen, *Nature* **387** (1997) 569
2. D. A. Brown, E. London, *Annu. Rev. Cell Dev. Biol.* **14** (1998) 111
3. M. Edidin, *Annu. Rev. Biophys. Biomol. Struct.* **32** (2003) 257
4. J. F. Hancock, *Nat. Rev. Mol. Cell Biol.* **7** (2006) 456
5. D. Marguet, P. F. Lenne, H. Rigneault, H. T. He, *EMBO J.* **25** (2006) 3446
6. K. Jacobson, O. G. Mouritsen, R. G. Anderson, *Nat. Cell Biol.* **9** (2007) 7
7. C. S. Flordellis, *Curr. Pharm. Des.* **18** (2012) 145
8. A. Pralle, P. Keller, E. L. Florin, K. Simons, J. K. Horber, *J. Cell Biol.* **148** (2000) 997
9. D. A. Zacharias, J. D. Violin, A. C. Newton, R. Y. Tsien, *Science* **296** (2002) 913
10. H. Niv, H. O. Gutman, Y. Kloog, Y. I. Henis, *J. Cell Biol.* **157** (2002) 865
11. I. A. Prior, C. Muncke, R. G. Parton, J. F. Hancock, *J. Cell Biol.* **160** (2003) 165
12. K. Gaus, E. Gratton, E. P. Kable, A. S. Jones, I. Gelissen, L. Kritharides, W. Jessup, *Proc. Natl. Acad. Sci. USA* **100** (2003) 15554
13. P. Sharma, R. Varma, R. C. Sarasij, Ira, K. Gousset, G. Krishnamoorthy, M. Rao, S. Mayor, *Cell* **116** (2004) 577
14. K. Bacia, D. Scherfeld, N. Kahya, P. Schwille, *Biophys. J.* **87** (2004) 1034
15. A. Ianoul, D. D. Grant, Y. Rouleau, M. Bani-Yaghoob, L. J. Johnston, J. P. Pezacki, *Nat. Chem. Biol.* **1** (2005) 196

16. M. J. Swamy, L. Ciani, M. Ge, A. K. Smith, D. Holowka, B. Baird, J. H. Freed, *Biophys. J.* **90** (2006) 4452
17. A. Fujita, J. Cheng, M. Hirakawa, K. Furukawa, S. Kusunoki, T. Fujimoto. *Mol. Biol. Cell* **18** (2007) 2112.
18. V. Vukojević, Y. Ming, C. D'Addario, M. Hansen, U. Langel, R. Schulz, B. Johansson, R. Rigler, L. Terenius. *FASEB J.* **22** (2008) 3537.
19. V. Vukojević, Y. Ming, C. D'Addario, R. Rigler, B. Johansson, L. Terenius. *PLOS ONE* **3** (2008) e4008
20. R. Kraut, N. Bag, T. Wohland. *Methods Cell Biol.* **108** (2012) 395.
21. P. Sengupta, T. Jovanovic-Talisman, D. Skoko, M. Renz, S. L. Veatch, J. Lippincott-Schwartz, *Nat. Methods* **8** (2011) 969
22. P. Sengupta, T. Jovanovic-Talisman, J. Lippincott-Schwartz, *Nat. Protoc.* **8** (2013) 345
23. V. Vukojević, A. Pramanik, T. Yakovleva, R. Rigler, L. Terenius, G. Bakalkin, *Cell. Mol. Life Sci.* **62** (2005) 535
24. E. L. Elson, *Methods Enzymol.* **518** (2013) 11
25. J. Ries J. P. Schwille, *Bioessays* **34** (2012) 361
26. D. Magde, W. W. Webb, E. Elson, *Phys. Rev. Lett.* **29** (1972) 705
27. M. Ehrenberg, R. Rigler, *Chem. Phys. Lett.* **14** (1972) 539
28. E. L. Elson, D. Magde, *Biopolymers* **13** (1974) 1
29. M. Ehrenberg, R. Rigler, *Chem. Phys.* **4** (1974) 390
30. D. E. Koppel, *Phys. Rev., A* **10** (1974) 1938
31. R. Rigler, Ü. Mets, J. Widengren, P. Kask, *Eur. Biophys. J.* **22** (1993) 169
32. M. Eigen, R. Rigler, *Proc. Natl. Acad. Sci. USA* **91** (1994) 5740
33. K. Weisshart, V. Jüngel, S. J. Briddon, *Curr. Pharm. Biotechnol.* **5** (2004) 135
34. V. Vukojević, M. Heidkamp, Y. Ming, B. Johansson, L. Terenius, R. Rigler, *Proc. Natl. Acad. Sci. USA* **105** (2008) 18176
35. R. Saxena, A. Chattopadhyay, *J. Neurochem.* **116** (2011) 726
36. K. Herrick-Davis, E. Grinde, A. Cowan, J. E. Mazurkiewicz, *Mol. Pharmacol.* **84** (2013) 630
37. N. L. Thompson, *Fluorescence Correlation Spectroscopy*, in: *Topics in Fluorescence Spectroscopy: Techniques*, Vol. 1, J. R. Lakowicz, Ed., Plenum Press, New York, USA, 1991, Ch. 6, p. 337
38. H. Qian, E. Elson, *Biophys. J.* **57** (1990) 375
39. P. Kask, K. Palo, D. Ullmann, K. Gall, *Proc. Natl. Acad. Sci. USA* **96** (1999) 13756
40. P. Kask, K. Palo, N. Fay, I. Brand, U. Mets, D. Ullmann, J. Jungmann, J. Pschorr, K. Gall, *Biophys. J.* **78** (2000) 1703
41. Y. Chen, J. D. Müller, P. T. C. So, E. Gratton, *Biophys. J.* **77** (1999) 553
42. L. N. Hillesheim, J. D. Müller, *Biophys. J.* **85** (2003) 1948
43. J. D. Müller, *Biophys. J.* **86** (2004) 3981
44. B. Wu, J. D. Müller, *Biophys. J.* **89** (2005) 2721
45. B. Wu, Y. Chen, J. D. Müller, *Biophys. J.* **91** (2006) 2687
46. E. Petrov, *Derivation of expressions for the FCS correlation function*, 2005, <http://www.onlinedegreediscussion.com/free-online-textbooks/fluorescence-correlation-spectroscopy/> (accessed in November, 2013)
47. P. Kapusta, *Absolute Diffusion Coefficients: Compilation of Reference Data for FCS Calibration*, PicoQuant Application Note 2010
48. L. Wawrezinieck, P. F. Lenne, D. Marguet, H. Rigneault, *Proc. SPIE Int. Soc. Opt. Eng.* (2004) 92

49. L. Wawrezinieck, L. H. Rigneault, D. Marguet, P. F. Lenne, *Biophys. J.* **89** (2005) 4029
50. P.-F. Lenne, L. Wawrezinieck, F. Conchonaud, O. Wurtz, A. Boned, X. J. Guo, H. Rigneault, H.-T. He, D. Marguet, *EMBO J.* **25** (2006) 3245
51. H.-T. He, D. Marguet, *Annu. Rev. Phys. Chem.* **62** (2011) 417
52. D. M. Owen, D. Williamson, C. Rentero, K. Gaus, *Traffic* **10** (2009) 962
53. J. Wenger, F. Conchonaud, J. Dintinger, J. L. Wawrezinieck, T. W. Ebbesen, H. Rigneault, D. Marguet, P.-F. Lenne, *Biophys. J.* **92** (2007) 913
54. E. Betzig, G. H. Patterson, R. Sougrat, O. W. Lindwasser, S. Olenych, J. S. Bonifacino, M. W. Davidson, J. Lippincott-Schwartz, H. F. Hess, *Science* **313** (2006) 1642
55. S. T. Hess, T. P. K. Girirajan, M. D. Mason, *Biophys. J.* **91** (2006) 4258
56. M. J. Rust, M. Bates, X. Zhuang, *Nat. Methods* **3** (2006) 793
57. X. Michalet, T. D. Lacoste, S. Weiss, *Methods* **25** (2001) 87
58. R. E. Thompson, D. R. Larson, W. W. Webb, *Biophys. J.* **82** (2002) 2775
59. A. Yildiz, J. N. Forkey, S. A. McKinney, T. Ha, Y. E. Goldman, P. R. Selvin, *Science* **300** (2003) 2061
60. J. Fölling, M. Bossi, H. Bock, R. Medda, C. A. Wurm, B. Hein, S. Jakobs, C. Eggeling, S. W. Hell, *Nat. Methods* **5** (2008) 943
61. R. Wombacher, M. Heidebreder, S. van de Linde, M. P. Sheetz, M. Heilemann, V. W. Cornish, M. Sauer, *Nat. Methods* **7** (2010) 717
62. G. H. Patterson, J. Lippincott-Schwartz, *Science* **297** (2002) 1873
63. M. R. T. Dale, P. Dixon, M.-J. Fortin, P. Legendre, D. E. Myers, M. S. Rosenberg, *Ecography* **25** (2002) 558
64. M. Scarselli, P. Annibale, A. Radenović, *J. Biol. Chem.* **287** (2012) 16768
65. D. Lando, U. Endesfelder, H. Berger, L. Subramanian, P. D. Dunne, J. McColl, D. Klenerman, A. M. Carr, M. Sauer, R. C. Allshire, M. Heilemann, E. D. Laue, *Open Biol.* **2** (2012) 120078
66. S. Malkusch, W. Muranyi, B. Muller, H. G. Krausslich, M. Heilemann, *Histochem. Cell Biol.* **139** (2013) 173
67. C. Coltharp, R. P. Kessler, J. Xiao, *PLOS ONE* **7** (2012) e51725
68. D. M. Owen, C. Rentero, J. Rossy, A. Magenau, D. Williamson, M. Rodriguez, K. Gaus, *J. Biophotonics* **3** (2010) 446
69. S. AbdAlla, H. Lothar, A. el Massiery, U. Qwitterer, *Nat. Med.* **7** (2001) 1003
70. A. Getis, J. Franklin, *Ecology* **68** (1987) 473
71. S. Manley, J. M. Gillette, J. Lippincott-Schwartz, *Nat. Methods* **5** (2008) 155
72. A. Sharonov, R. M. Hochstrasser, *Proc. Natl. Acad. Sci. USA* **103** (2006) 18911
73. G. Giannone, E. Hosy, F. Levet, A. Constals, K. Schulze, A. I. Sobolevsky, M. P. Rosconi, E. Gouaux, R. Tampe, D. Choquet, L. Cognet, *Biophys. J.* **99** (2010) 1303
74. P. Annibale, S. Vanni, M. Scarselli, U. Rothlisberger, A. Radenovic, *Nat Methods* **8** (2011) 527
75. P. Annibale, S. Vanni, M. Scarselli, U. Rothlisberger, A. Radenovic, *PLOS ONE* **6** (2011) e22678
76. V. Katritch, V. Cherezov, R. C. Stevens, *Annu. Rev. Pharmacol. Toxicol.* **53** (2013) 531
77. G. Liapakis, A. Cordomi, L. Pardo, *Curr. Pharm. Des.* **18** (2012) 175
78. X. Deupi, B. K. Kobilka, *Physiology (Bethesda)* **25** (2010) 293
79. T. Kenakin, *J. Recept. Signal. Transduct. Res.* **30** (2010) 313
80. T. Wohland, K. Friedrich, R. Hovius, H. Vogel, *Biochemistry* **38** (1999) 8671

81. R. Rigler, A. Pramanik, P. Jonasson, G. Kratz, O. T. Jansson, P. Nygren, S. Ståhl, K. Ekberg, B. Johansson, S. Uhlén, M. Uhlén, H. Jörnvall, J. Wahren, *Proc. Natl. Acad. Sci. USA* **96** (1999) 13318
82. R. C. Patel, U. Kumar, D. C. Lamb, J. S. Eid, M. Rocheville, M. Grant, A. Rani, T. Hazlett, S. C. Patel, E. Gratton, Y. C. Patel, *Proc. Natl. Acad. Sci. USA* **99** (2002) 3294
83. N. Kahya, D. A. Wiersma, B. Poolman, D. Hoekstra, *J. Biol. Chem.* **277** (2002) 39304
84. R. C. Calizo, S. Scarlata, *Anal. Biochem.* **440** (2013) 40
85. K. Herrick-Davis, E. Grinde, T. Lindsley, A. Cowan, J. E. Mazurkiewicz, *J. Biol. Chem.* **287** (2012) 23604
86. L. E. Kilpatrick, S. J. Briddon, N. D. Holliday, *Biochim. Biophys. Acta* **1823** (2012) 1068
87. R. H. Rose, S. J. Briddon, S. J. Hill, *Br. J. Pharmacol.* **165** (2012) 1789
88. S. Ganguly, A. Chattopadhyay, *Biophys. J.* **99** (2010) 1397
89. L. Milan-Lobo, I. Gsandtner, E. Gaubitzer, D. Rünzler, F. Buchmayer, G. Köhler, A. Bonci, M. Freissmuth, H. H. Sitte, *Mol. Pharmacol.* **76** (2009) 1196
90. B. Ilien, B. N. Glasser, J. P. Clamme, P. Didier, E. Piemont, R. Chinnappan, S. B. Daval, J. L. Galzi, Y. Mely, *J. Biol. Chem.* **284** (2009) 19533
91. M. Triantafilou, P. M. Lepper, C. D. Briault, M. A. Ahmed, J. M. Dmochowski, C. Schumann, K. Triantafilou, *Eur. J. Immunol.* **38** (2008) 192
92. Y. Cordeaux, S. J. Briddon, S. P. Alexander, B. Kellam, S. J. Hill, *FASEB J.* **22** (2008) 850
93. F. Philip, P. Sengupta, S. Scarlata *J. Biol. Chem.* **282** (2007) 19203
94. R. J. Middleton, S. J. Briddon, Y. Cordeaux, A. S. Yates, C. L. Dale, M. W. George, J. G. Baker, S. J. Hill, B. Kellam, *J. Med. Chem.* **50** (2007) 782
95. O. Hegener, L. Prenner, F. Runkel, S. L. Baader, J. Kappler, H. Häberlein, *Biochemistry* **43** (2004) 6190
96. M. Scarselli, P. Annibale, C. Gerace, A. Radenovic, *Biochem. Soc. Trans.* **41** (2013) 191.